Q. J. R. Meteorol. Soc. (2000), **126**, pp. 001–999

Teleconnections and low frequency variability in idealized experiments with two storm tracks

By Christian Franzke, Klaus Fraedrich* and Frank Lunkeit

Meteorologisches Institut, Universität Hamburg, Germany

(Received July 2000; revised November 2000)

SUMMARY

Low frequency variability and teleconnection patterns induced by two storm tracks in idealized experiments depend on their zonal distance. A separation of about 150°, which resembles the Northern Hemisphere storm track distribution, reveals teleconnection patterns which are similar to the PNA and NAO. The NAO-like structure is associated with retrograde travelling Rossby waves; barotropic streamfunction tendencies show that the interaction of the stationary eddies with the low frequency flow and the high frequency eddies contribute to the amplification of the pattern. Its decay is due to their interaction with the zonal mean flow, and the low frequency contribution to the divergence term. The PNA-like pattern has a longer memory and is linked to a quasi-stationary wave. The stationary wave activity flux shows the dominating influence of baroclinic processes and the other storm track further upstream. The correlation between the teleconnection indices is significant for storm track distances between 180° and 160°, and vanishes between 150° and 130°.

KEYWORDS: Idealized experiments Low frequency variability Storm track interaction Teleconnection

1. Introduction

One interesting phenomenon of the atmosphere's midlatitude low frequency variability is the fact that a large amount of its variance can be described by a few geographically fixed circulation regimes as, for example, the Pacific-North American pattern and the North Atlantic Oscillation (PNA and NAO, Wallace and Gutzler 1981). These teleconnection patterns describe standing waves oscillating with time scales of a month or longer. Blackmon et al. (1984a, 1984b) have investigated pronounced teleconnection patterns and their time evolution on different time scales. For long time scales (periods much longer than a month) they find meridionally oriented dipole structures in the storm track regions, whereas the patterns of intermediate periods between 10 and 30 days consist of zonally oriented wave trains, developing in the jet entrance regions and propagating into the tropics after crossing the storm track regions. Another distinction is that the long time scale patterns are regionally fixed, whereas the intermediate time scale patterns show a Rossby wave dispersion along geographically fixed wave guides.

In a modeling study Feldstein (1998) shows that low frequency anomalies undergo their complete life cycle in 10-11 days, and in an observational study (Feldstein 2000) he shows that the PNA life-cycle is complete in less than 15 days. Therefore, Feldstein concludes, averaging over monthly or seasonal time scales can lead to misinterpretations of the dynamics of low frequency anomalies. Though the time scales of the life cycles of the low frequency variability is, in general, shorter than a month, the monthly mean flow with its low frequency anomaly is different from the climatology itself. Therefore, these low frequency anomalies induce variability on different time scales. Frederiksen (1983), Simmons et al. (1983) and Blackmon et al. (1984b) relate the long time scale patterns (longer than a month) to the fastest growing mode associated with barotropic instability in zonally asymmetric time mean flows. Feldstein (2000) associates the growth of the PNA with the interaction between the anomaly and the time-mean zonally asymmetric

* Corresponding author: Meteorologisches Institut, Universität Hamburg, Bundesstrasse 55, D-20146 Hamburg, Germany, E-mail: fraedrich@dkrz.de

flow and wave dispersion.

The interaction between the Atlantic and the Pacific regions is another feature to be analysed. Winter climate anomalies show that, during anti-cyclonic (cyclonic) situations in Europe, the Atlantic storm track intensity is enhanced (reduced) and its end is shifted northward (remains zonal), which is connected with a further (less) eastward extension of the North Pacific storm track (Fraedrich et al. 1993, supported by Sickmöller et al. 2000, analysing cyclone tracks). A correlation (-0.42) between PNA and NAO index time series is found by Bongioannini-Cerlini et al. (1999), indicating a hemispheric coherence in the atmospheric circulation. By using the multichannel version of the singular spectrum analysis Plaut and Vautard (1994) detect 30-60 day oscillating modes in the Atlantic and the Pacific region which are uncorrelated. They further observe a hemispheric 40-45 day oscillation with patterns which are regionally similar to the 30-60 day modes. By examining positive amplitude events, they find that the hemispheric oscillation consists of two different oscillations, whose phases are locked intermittently. Lejenäs and Økland (1983) do not discover a connection between the blocking events in the two regions.

The motivation for this study is to investigate the interaction and low frequency variability of two storm tracks in idealized experiments. For this purpose sensitivity experiments are carried out with different zonal distances between the two storm tracks. Teleconnection patterns and index time series are calculated for both regions to display and compare the variability. Insight into the underlying dynamics is gained through the streamfunction tendency equation and the three-dimensional wave activity flux. Section 2 describes the model and the experimental design. The climatology of the low frequency variability follows in section 3 and the dynamics of the variability is discussed in section 4. The paper closes with a summary and the conclusions.

2. Model description and experimental design

Storm track experiments are performed with the simplified GCM PUMA (Portable University Model of the Atmosphere, Fraedrich et al. 1998), which is a global spectral model (Hoskins and Simmons 1975, James and Gray 1986) solving the primitive equations on sigma levels. The diabatic and dissipative processes are represented through Newtonian cooling and Rayleigh friction (James and Gray 1986, Held and Suarez 1994). PUMA is used with T21 truncation and 5 equally spaced sigma levels. Simplified GCM's have been applied to idealized studies of low frequency variability and storm track characteristics by James and James (1992), James et al. (1994), Frisius et al. (1998), Lunkeit et al. (1998), Franzke et al. (2000) and Walter et al. (2000).

The diabatic heating is parameterized by a restoration temperature T_R, the model temperature T and the relaxation time scale τ_R:

$$\left(\frac{\partial T}{\partial t}\right)_{diab.} = \frac{T_R - T}{\tau_R}. \tag{1}$$

Thus, the model is driven by relaxation of its temperature towards the restoration temperature. The relaxation time scale τ_R is 5 days in the lowest layer, 10 days at the second and 30 days at the three remaining upper layers. The Rayleigh friction time scale is one day in the lowest layer and there is no friction at all other layers. The Newtonian cooling and Rayleigh friction time scales are chosen to ensure the development of realistic storm track characteristics (Frisius et al. 1998).

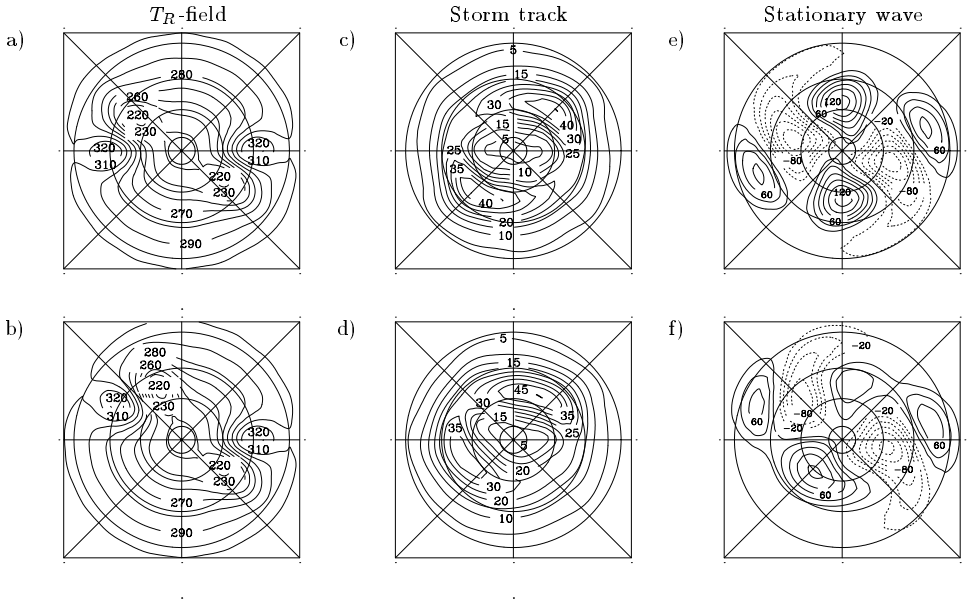

Figure 1. Restoration temperature on 900 hPa (contour interval is 10 K) for a) 180°, b) 150° T_R-dipole separation; standard deviation of band pass filtered 500 hPa geopotential (contour interval is 5 gpm) for c) 180°, d) 150°; long term mean of 300 hPa geopotential minus zonal mean (contour interval is 20 gpm, negative values are dashed, the zero contour is not displayed) for e) 180°, f) 150°.

A zonally symmetric restoration temperature field is superimposed by a zonally asymmetric contribution consisting of two idealized temperature dipoles (Fig. 1a and b). The warm pole situated upstream and south of the cold pole, idealizes a warm ocean (representing the Gulf stream or the Kuroshio) while the cold pole represents a cold continent (North America or Asia). The amplitude of the restoration temperature dipoles decreases with height, vanishing at the tropopause, which is the highest sigma level (Fraedrich et al. 1998). In sensitivity experiments the zonal distance between the two restoration temperature dipoles is changed in 5° steps from 180° to 130° (see schematic diagram, Fig. 2); the distance remains fixed during a sensitivity experiment. The area downstream of the shifted dipole is called the A-area, the other is defined as P-area. The meridian through the center of the warm pole part of the fixed dipole is referred to as 0°E. The cases of a zonal distance of 180° and 150° are shown in Fig. 1a and b. Note that a separation of about 150° resembles the geographical distribution of the Northern Hemisphere storm tracks. The model is started from a resting atmosphere and the surface pressure is initialized by a small disturbance. All experiments run for 101 years in a perpetual mode; the evaluation of the first year is omitted because of the spin-up time of the model.

3. Climatology of the low frequency variability

The influence of the zonal distance between two storm tracks on the low frequency variability, the teleconnection and their interaction is demonstrated by comparing the 180°-experiment with sensitivity experiments of varying zonal distance, where the emphasis lies on the 150° dipole separation. First, the climatology is presented, followed by the description of teleconnection patterns and their interaction.

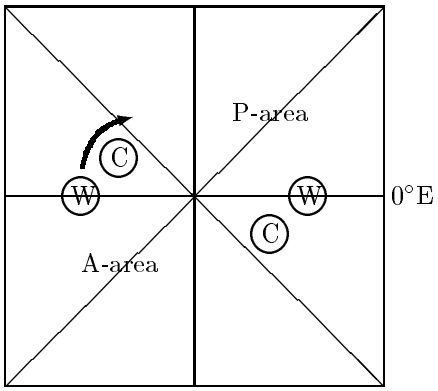

Figure 2. Schematic diagram of the shift of the dipole in the sensitivity experiments. During the respective experiments they remain fixed. C and W indicate the cold and warm poles.

(*a*) *Climatological setting: transient and stationary eddies*

The climatology of the experiments reveals the main characteristics of the observed midlatitude Northern Hemisphere circulation. The *transient eddies* (Fig. 1c and d) which are measured by the standard deviation of the band pass filtered 500 hPa geopotential (periods between 2-8 days, Trenberth 1991) represent storm tracks. Their structure, intensity and position relative to the jets (not shown) are comparable with observations (Lau 1988). The 180°-experiment shows two storm tracks of equal intensity and shape. The 150°-experiment reveals a stronger storm track in the P-area than in the A-area (Fig. 1d); the P-storm track (A-storm track) is also stronger (weaker) than in the 180°-experiment, which indicates the influence of the global stationary wave field on the distribution of the baroclinicity (not shown) and, therefore, on the storm track intensity. The *stationary eddies* (Fig. 1e and f) represent the time mean zonal deviation of the 300 hPa geopotential: A positive monopole anomaly occurs at the end of a storm track, with a lower-level through and an upper-level ridge east of a warm pole representing the baroclinic response to midlatitude heating (Walter et al. 2000). A dipole-like pattern appears at its beginning, which is associated with the restoration temperature dipole (Fig. 1a and b) where high values are located over the warm pole (and vice versa). Note that these dipole-like stationary patterns deflect equatorwards near the T_R-dipole of the other storm track. The stationary wave patterns are less pronounced in the 150°-experiment; in particular, the wave train starting in the P-area is less intense and shows a shorter arc towards the equator.

(*b*) *Teleconnections*

Teleconnection patterns are centers of action which characterize low frequency variability of atmospheric fields between remote locations. Following Wallace and Gutzler (1981) they are deduced from the correlation matrix, whose elements are the temporal correlation coefficients, r_{ij}, between monthly mean 300 hPa geopotential fluctuations, Φ_i', at any selected grid point (subscript i) and every other grid point (subscript j); the

primes denote deviations from the time mean indicated by bars:

$$r_{ij} = \frac{\overline{\Phi_i{}' \Phi_j{}'}}{\sqrt{\overline{\Phi_i{}'^2}}\sqrt{\overline{\Phi_j{}'^2}}}. \tag{2}$$

The centers of action inducing low-frequency variability are identified by the teleconnectivity, given by the (negative) correlation minimum of each column of the correlation matrix:

$$T_i = |(r_{ij}) \text{ minimum for all j } | . \tag{3}$$

In all experiments large values of teleconnectivity occur in the storm track areas downstream of the T_R-dipoles. The 180°-experiment shows three centers of action in both storm track areas (Fig. 3a); in the 150°-experiment the high teleconnectivity extends over large areas (Fig. 3b).

Teleconnection patterns (A and P): Teleconnection patterns are defined by the columns of the correlation matrix which, spatially displayed, represent one-point correlation maps. To compare the patterns induced by different storm track separations, the same base points are chosen for all sensitivity experiments; they are located where nearly the highest teleconnectivity occurs in all experiments. In the P-area this base point is situated at 56.3°E, 47.1°N and, for the A-area, the position is 230.6°E, 47.1°N. The teleconnection patterns are presented for the 180° and 150°-experiment: (i) In the 180°-experiment the one-point correlation maps reveal south-eastward travelling wave trains starting in the centers of the storm tracks (Fig. 3c and e). These patterns look like the first complex empirical orthogonal function (CEOF) of the vertical mean streamfunction (Franzke et al. 2000), which is associated with a retrograde travelling Rossby wave consisting both of a 50 days travelling and a 50 days amplitude modulation period. (ii) In the 150°-experiment a quadrupole pattern develops in the P-area (Fig. 3d) which is centered in the storm track. It describes an arc which originates in the sub-tropics (south of the warm part of the T_R-pole), extends to the northeast and turns southward into the sub-tropics near the end of the storm track (P-pattern). In the A-area, the one-point correlation map is a dipole pattern with a southwest-northeast axis describing a meridional sea saw (A-pattern). Summarizing, two teleconnection patterns, which are similar to the Pacific-North American pattern (PNA or, in our case, the P-pattern) and the North Atlantic Oscillation (NAO, or the A-pattern), develop in a flow induced by quite a realistic spatial distribution of the storm tracks forced by diabatic heating dipoles. That is, the spatial structure of the low-frequency variability, like the PNA and NAO, is largely governed by the stationary wave fields linked to the storm tracks and their positions.

(*c*) *Space-time variability*

The space-time variability of the upper layer geopotential height field (300 hPa) is analysed to characterize the evolution of the individual P- or A-patterns, to determine their wave propagation properties by daily one-point lag-correlations, and to describe the temporal correlation between them.

Daily lag-correlation maps: One-point lag-correlations of the low-pass filtered 300 hPa geopotential fluctuations (periods > 10 days, the time mean is subtracted, Blackmon 1976, Blackmon et al., 1984b) yield the following space-time variability: The 180°-experiment is associated with a retrograde travelling Rossby wave (not shown, see Franzke et al. 2000). The 150°-experiment (Fig. 4) reveals that the teleconnection patterns appear with

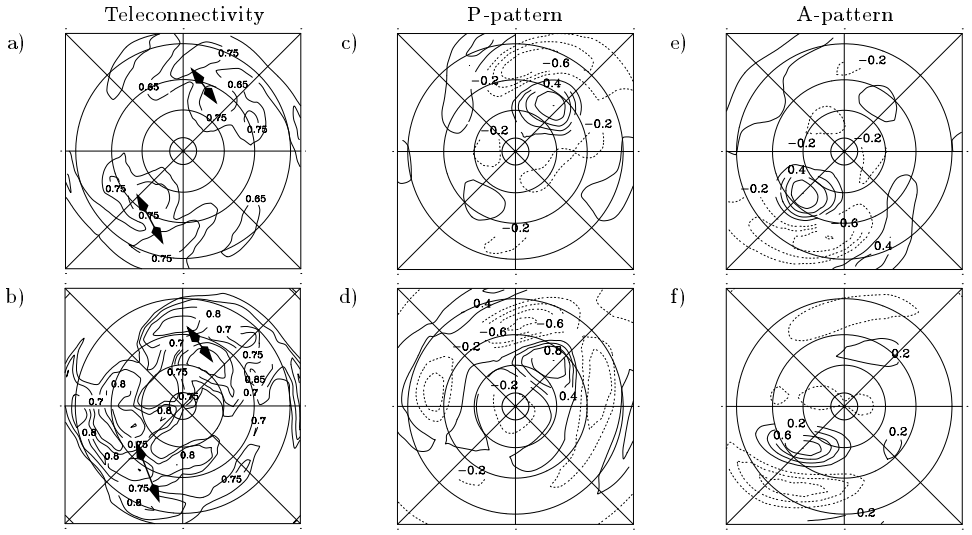

Figure 3. Teleconnectivity (contour interval is 0.05) of monthly mean 300 hPa geopotential for a) 180° and b) 150° T_R-dipole separation. Local correlations of monthly mean 300 hPa geopotential (contour interval is 0.2, negative values are dashed, the zero contour is not displayed): base point 56.3°E, 47.1°N: c) 180° and d) 150°; base point 230.6°E, 47.1°N: e) 180° and f) 150°.

similar patterns as in the monthly mean data and can be interpreted as standing waves. Both A- and P-areas show downstream amplification of the centers of action (stationary correlation extrema). That is, the wave energy disperses along an arc extending over the respective downstream ends of the storm tracks into the sub-tropics. As the A- and P-patterns occur in the vicinity of the storm tracks, the storm track dynamics is linked to them, as demonstrated below. The corresponding teleconnection patterns based on low pass filtered data at zero-lag are less pronounced than the patterns based on monthly means.

Daily teleconnection index: A daily teleconnection index is defined as the difference of normalized fluctuations between two anti-correlated regions, region-1 and region-2, (subscript '1' and '2') averaged over four grid points. It is introduced to further investigate the space-time behaviour of the teleconnection patterns:

$$Index = \left(\frac{1}{4} \sum_{n=1}^{4} \frac{\Phi_n{}'}{\sqrt{\overline{\Phi_n{}'^2}}} \right)_1 - \left(\frac{1}{4} \sum_{m=1}^{4} \frac{\Phi_m{}'}{\sqrt{\overline{\Phi_m{}'^2}}} \right)_2 . \tag{4}$$

The A-index is defined by averaging over region-1 ($47.1 - 41.5°$N, $230.6 - 236.2°$E) and region-2 ($24.9 - 19.4°$N, $247.5 - 253.1°$E), the P-index over region-1 ($47.1 - 41.5°$N, $56.3 - 61.9°$E) and region-2 ($30.5 - 24.9°$N, $90.0 - 95.6°$E). Both time series are normalized by the standard deviation.

Spectral analysis (see for example von Storch and Zwiers 1998) of both the P- and A-index for the 180°-experiment reveals a pronounced peak at a period of about 50 days without phase lag which is due to the dominating retrograde travelling Rossby wave of 50 day period (not shown, see Franzke et al. 2000). The 150°-experiment does not exhibit the pronounced 50 day period observed in the 180°-experiment so that both indices can

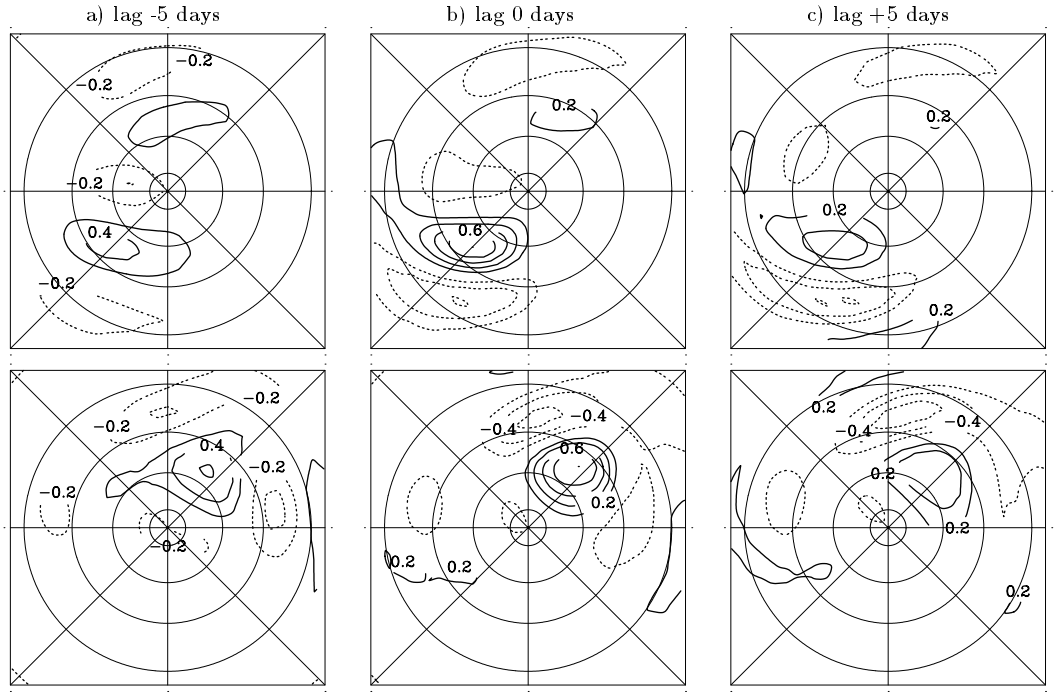

Figure 4. 150°-experiment: Lag correlation patterns of 300 hPa geopotential height for the A-area (upper row) and the P-area (lower row) based on low pass filtered daily data for lags (relative to the time series at the base point) of -5 days (a), 0 days (b) and +5 days (c) (the contour interval is 0.2, the zero contour is not displayed).

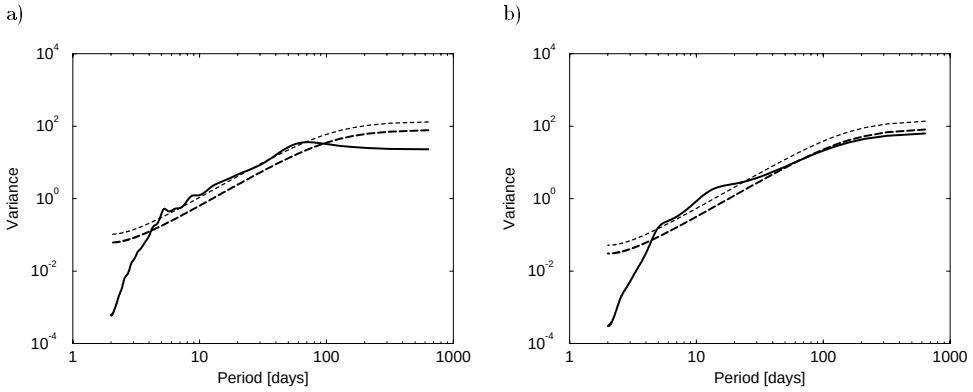

Figure 5. 150°-experiment: Variance spectra of a) A-index, and b) P-index (in $1m^2s^{-4}$, the equivalent first order autoregressive process AR(1) is indicated by a dashed line, the 99% confidence limit is indicated by a dotted line).

Dipole separation	correlation	e-folding time-scale	
		P-area	A-area
180°	+0.332	7	8
175°	+0.346	9	9
170°	+0.348	10	9
165°	+0.338	10	8
160°	+0.258	9	9
155°	+0.154	4	5
150°	+0.032	20	9
145°	+0.034	5	6
140°	+0.014	9	10
135°	-0.023	5	6
130°	+0.003	7	8

TABLE 1. Correlation between A- and P-index in the respective experiments and e-folding time-scale (in days) of the teleconnection indices.

be represented by red noise spectra (or the equivalent first order autoregressive process AR(1), Fig. 5). Note that there is an increase of A- and P-index variance for periods between 3 and 20 days and, for the A-index, also around 50 days, which are slightly above the 99% confidence limit of the equivalent AR(1)-spectra. A *time-scale* of the daily index (Tab. 1) is defined by the e-folding decay time of the autocorrelation of the index time-series. For all sensitivity experiments both indices show almost the same memory with about 8 days. In the 150°-experiment, the P-index has a large e-folding time-scale of about 20 days compared to the A-index with 9 days.

The *co-spectra* between the A- and P-index change with the zonal distance between the two storm tracks. They range from a high coherence for the 180°-experiment, where they are in phase with each other, to unsignificant coherences in the 130°-experiment (not shown). The *correlation* between both indices reduces with decreasing zonal separation (Tab. 1): The correlation remains roughly constant (about 0.3 with 99% significance) for zonal distances between 180° and 165°; it vanishes after further decreasing the separation. That is, a transition occurs at the 155° storm track separation changing from a flow dominated by zonal wavenumber two (Franzke et al. 2000, analyzing the 180°-experiment) to uncorrelated and localized structures in both storm track regions.

4. Dynamics of the low frequency variability

The evolution of the anomalous flow associated with the teleconnection pattern is represented (a) by life-cycle composites of the vertical mean streamfunction anomaly, which are linked to teleconnection index extremes and, to gain insight into the dynamics, analysed by (b) the vertical mean streamfunction tendency and (c) the three-dimensional wave activity fluxes.

(*a*) *Barotropic flow composites*

In the 180°-experiment Franzke et al. (2000) have constructed life-cycle composites linked to the maximum amplitude of the first complex empirical orthogonal function (CEOF) of the vertical mean streamfunction. A CEOF-analysis is a tool to identify travelling patterns in time series. Subsequent analysis of streamfunction tendency terms shows that the variability of the flow is largely governed by the barotropic dynamics of a retrograde travelling Rossby wave. However, as CEOFs of the 150°-experiment do not reveal preferred propagation periods, the patterns of the CEOFs cannot be associated

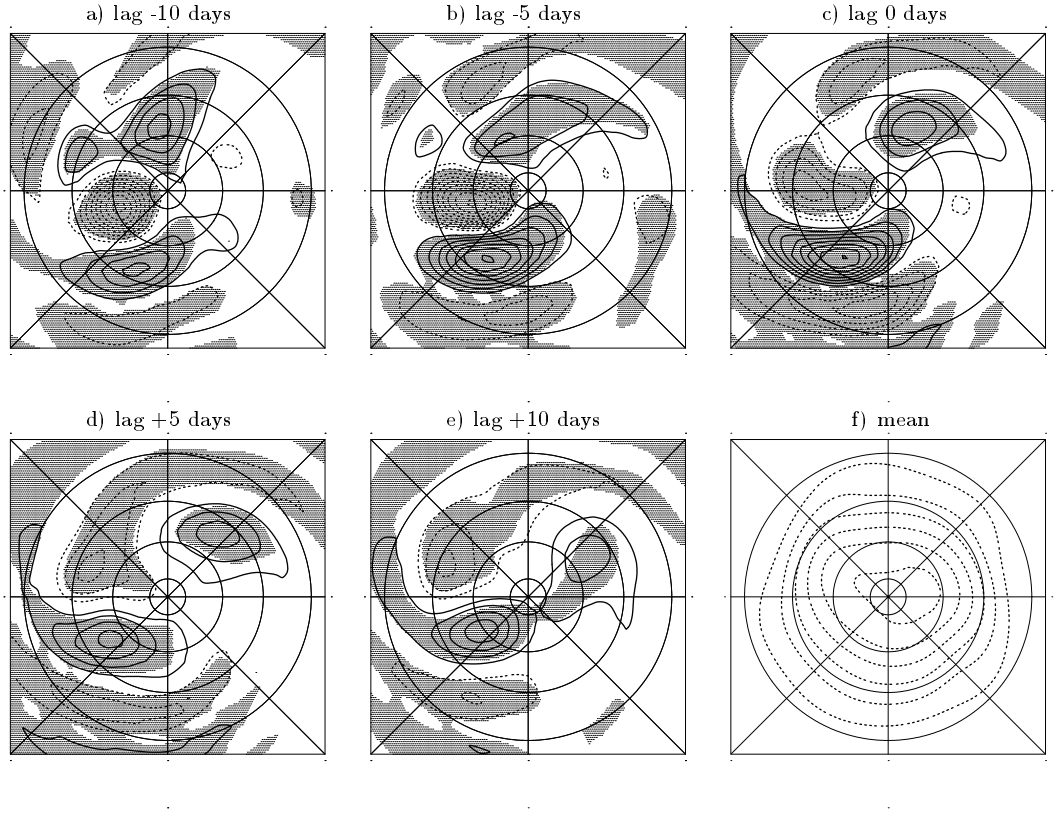

Figure 6. 150°-experiment (A-area): Composites of the vertical mean streamfunction anomaly for positive A-index events at a) day -10, b) day -5, c) day 0, d) day 5, e) day 10 (contour interval is $5 \cdot 10^5 m^2 s^{-1}$, shading indicates significance above the 99%-level) and f) the vertically averaged time-mean streamfunction (contour interval is $10^7 m^2 s^{-1}$, negative isolines are dashed).

with travelling waves, and dynamic analysis based on CEOFs is not appropriate in this case. Therefore, the daily P- and A-index time series (introduced in section 3) are used instead to derive life-cycle composites. These life-cycle composites are centered (zero-lag) on the extremes of a teleconnection index spanning twenty days before and after. Note that reanalysis of the 180°-experiment with the teleconnection indices, instead of the complex principal components of the CEOF, does not change the results.

The life-cycle composites of the 150°-experiment show the following results: (i) A positive *A-index* is associated with a retrograde travelling Rossby wave (Fig. 6). It originates in the center of the A-storm track at the (-20 day)-lag (not shown) and propagates downstream. When the high pressure area of this wave passes the storm track, its amplitude amplifies (until zero-lag) and decays afterwards. This storm track induced amplification of the anti-cyclonic part of the wave is similar to the 'spatial resonance' mechanism introduced by Franzke et al. (2000) for the 180°-experiment. Note that at zero-lag the high pressure area of the barotropic wave composite has the same position as the positive area of the one point correlation map (Fig. 3f), whereas the center of the low pressure area (further downstream) does not coincide with the negative area in the one point correlation map

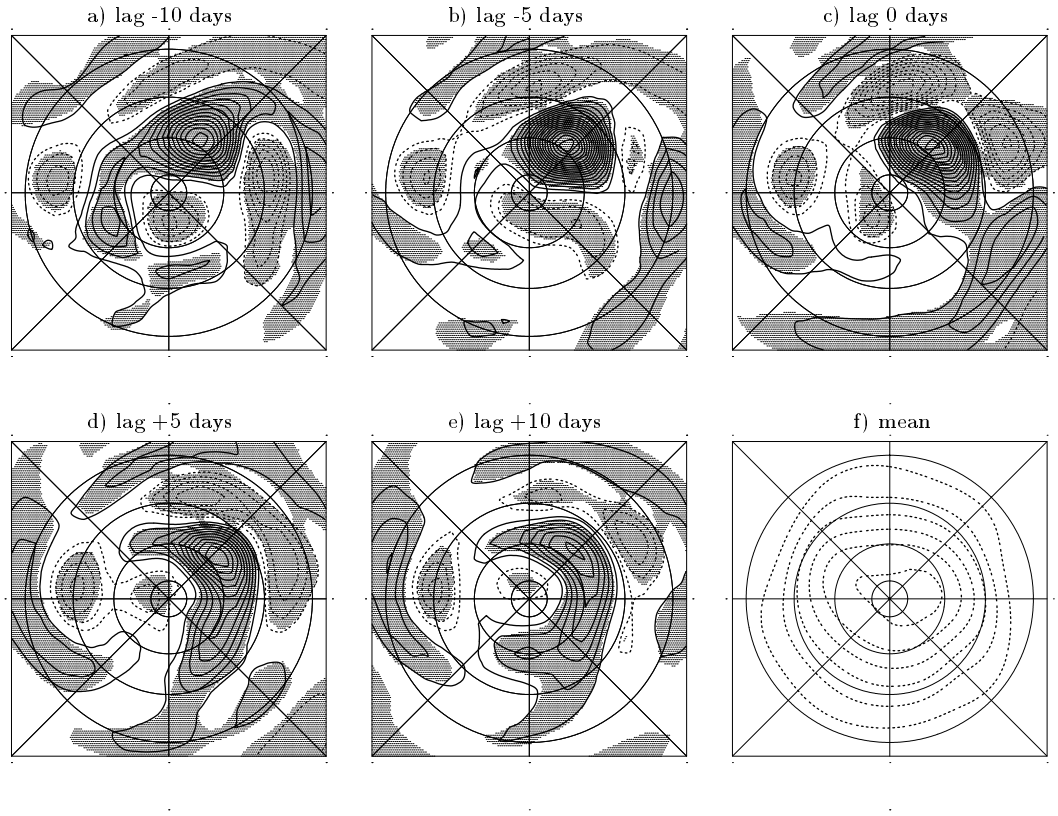

Figure 7. 150°-experiment (P-area): Composites of the vertical mean streamfunction anomaly for positive P-index events at a) day -10, b) day -5, c) day 0, d) day 5, e) day 10 (contour interval is $5 \cdot 10^5 m^2 s^{-1}$, shading indicates significance above the 99%-level) and f) the vertically averaged time-mean streamfunction (contour interval is $10^7 m^2 s^{-1}$, negative isolines are dashed).

but is shifted eastward. The system decays after zero-lag. (ii) A large positive *P-index* shows a different behaviour of the barotropic wave, which is stationary. The center of the positive anomaly remains at the same position during the composite life cycle (Fig. 7). It amplifies until zero-lag and decays thereafter with an upstream development, indicating a wave dispersion which resembles the life-cycle of a persistent blocking event. The results obtained for the negative phase of the indices are similar to those of the positive phase but with the opposite signs (not shown).

(*b*) *Barotropic streamfunction tendency*

The processes underlying the dynamically different behaviour observed in the A-domain and the P-domain are analysed by the streamfunction tendency which contains eight terms χ_i besides the residual R (Cai and van den Dool 1994, Feldstein 1998):

$$\frac{\partial \psi^L}{\partial t} = \sum \chi_i + R. \tag{5}$$

In the following introduction of the eight forcing terms, the superscripts L and B refer to low pass (periods $>$ 10 days, Blackmon 1976) and band pass (2-8 days, Trenberth 1991)

filtered quantities (the time mean is subtracted), the overbar defines a 10 year mean, and the prime denotes deviations from the time mean. The bracket indicates zonal averaging and the asterisk the deviations from the zonal mean, ψ is streamfunction, ζ is vorticity, t is time, $\vec{u}$ is the horizontal wind vector, ω is the vertical velocity, $\vec{k}$ is the vertical vector component, p is pressure, and f is the Coriolis parameter; $\nabla\cdot$ is the divergence operator, $\nabla\times$ the rotation operator, and ∇^{-2} denotes the inverse Laplacian. The χ_i are written as:

$$
\begin{aligned}
\chi_1 &= \nabla^{-2}\left(-\vec{u}^L\cdot\nabla f\right)\\
\chi_2 &= \nabla^{-2}\left(-\left[\overline{\vec{u}}\right]\cdot\nabla\zeta^L-\vec{u}^L\cdot\nabla\left[\overline{\zeta}\right]\right)\\
\chi_3 &= \nabla^{-2}\left(-\overline{\vec{u}^*}\cdot\nabla\zeta^L-\vec{u}^L\cdot\nabla\overline{\zeta^*}\right)\\
\chi_4 &= \nabla^{-2}\left(-\left(f+\overline{\zeta}\right)\nabla\cdot\vec{u}^L-\zeta^L\nabla\cdot\overline{\vec{u}}\right)\\
\chi_5 &= \nabla^{-2}\left(-\left(\nabla\cdot\left(\vec{u}^L\zeta^L\right)\right)^L\right)\\
\chi_6 &= \nabla^{-2}\left(-\left(\nabla\cdot\left(\vec{u}^B\zeta^B\right)\right)^L\right)\\
\chi_7 &= \nabla^{-2}\left(-\left(\nabla\cdot\left(\vec{u}^L\zeta^B\right)\right)^L-\left(\nabla\cdot\left(\vec{u}^B\zeta^L\right)\right)^L\right)\\
\chi_8 &= \nabla^{-2}\left(-\vec{k}\cdot\left(\nabla\times\left(\omega^L\frac{\partial\overline{\vec{u}}}{\partial p}+\overline{\omega}\frac{\partial\vec{u}^L}{\partial p}+\omega'\frac{\partial\vec{u}'}{\partial p}\right)^L\right)\right).
\end{aligned}
\tag{6}
$$

The χ_i-terms are the planetary vorticity advection by the low frequency flow χ_1, the interaction between the zonal mean (zonally asymmetric) time mean flow with the low frequency flow χ_2 (χ_3), the low frequency contribution to the divergence term χ_4; the self interaction among the low frequency (high frequency) eddies, χ_5 (χ_6), the interaction between the low and high frequency eddies, χ_7, and the sum of the tilting terms and the vertical vorticity advection, χ_8.

Analysis: The influence of the forcing or damping terms of (5) is evaluated in the following using cross-spectral analysis and composite techniques. The time evolutions of the individual vertically averaged forcing terms χ_i affect the teleconnection patterns (section 3b). Thus each forcing term is projected on the teleconnection correlation patterns (A-pattern and P-pattern in Fig. 3d and f) which, written symbolically, is

$$
s_i = <\text{Teleconnection Pattern}>\cdot\chi_i. \tag{7}
$$

First, the resulting normalized time series s_i are compared with the corresponding time series of the daily teleconnection A-index and P-index by cross-spectral analysis (von Storch and Zwiers 1998). The spectra are interpreted in the following way: Amplifying the A- or P-index requires the scalar time series, derived from the projection of the respective forcing terms onto the A- or P-pattern, to lead the A- or P-index by a $0^\circ - 90^\circ$ phase, otherwise the index is weakened. Furthermore, the time series have to be coherent, for the forcing terms to contribute to the index amplification or decay. The space-time distribution (and influence) of the forcing terms is displayed by composites relative to their maximum effect on the patterns, that is $\max(s_i)$.

A-area: The *time* development of the contribution of the individual forcing terms to the A-index time series is interpreted by cross-spectral analysis and shows the following results in the 30-100 day period range (Tab. 2): (i) Projected onto the A-pattern, the contribution, χ_3 (Fig. 8c), is the leading forcing term because it leads the A-index phase

by about 60°. This term describes the interaction between the zonally asymmetric time mean flow (stationary waves) with the travelling low frequency waves (Cai and van den Dool 1994) and/or the barotropic instability (Frederiksen 1983, Simmons et al. 1983, Branstator 1990, 1992). The planetary vorticity advection by the low frequency flow, χ_1 (Fig. 8a), and the self interaction among the high frequency eddies, χ_6 (Fig. 8e), are leading the A-index by about 45°. (ii) Damping terms are the relative vorticity advection by the zonally symmetric time mean flow, χ_2(Fig. 8b), and the low frequency contribution to the divergence term, χ_4, (Fig. 8d), because both terms lag the A-index by a phase of about 135° and, thus, contribute to the decay of the A-index. All remaining terms, the projections of the self interaction among the low frequency eddies χ_5 (not shown), the interaction between the low and high frequency eddies χ_7 (not shown), and the sum of the tilting terms and the vertical vorticity advection, χ_8 (not shown), do not show a significant coherence with the A-index and, therefore, they do not contribute to the A-index variability.

The *spatial* distribution of the forcing terms is displayed by composites (Fig. 9) relative to the maximum projection of the respective forcing terms onto the A-pattern. The following results are noted: (i) The interaction between the zonally asymmetric time mean flow with the low frequency flow, χ_3, has its maximum forcing area in the positive part of the A-pattern, so that this term leads to an intensification of the barotropic wave (Fig. 9c). The planetary vorticity advection by the low frequency flow, χ_1, shows an area of maximum positive values at the end of the storm track which, further downstream reveals a comparatively weaker negative forcing region (Fig. 9a). This term leads to the observed retrograde motion of the barotropic wave (Fig. 6). The self interaction among the high frequency eddies, χ_6, has a dipole structure in the storm track region (Fig. 9e), where the positive forcing projects on the high of the barotropic wave, and the negative forcing onto the low (Fig. 6c), thus amplifying the wave. (ii) The interaction between the zonally symmetric time mean flow with the low frequency flow, χ_2, occupies a negative forcing region at the end of the storm track, followed upstream by a positive region and further upstream again a positive forcing area (Fig. 9b). This structure causes a progressive motion of the barotropic wave (Fig. 6) which is supported by the low frequency contribution to the divergence term, χ_4 (Fig. 9d), consisting of a negative forcing area slightly upstream of the center of the A-pattern (Fig. 3f). Thus the decay of the pattern is accomplished. In summary, the variability of the A-index is associated with a retrograde barotropic wave and initiated by the interaction between the zonally asymmetric time mean flow and the low frequency flow, χ_3. Amplification is enforced by the high frequency eddy forcing, χ_6 and propagation is due to the planetary vorticity advection, χ_1. The damping is initiated through progressive motion induced by the relative vorticity advection of the zonal symmetric time mean flow, χ_2, and the divergence term, χ_4.

P-area: The *time* development of the contribution of the individual forcing terms to the P-index time series shows a different behaviour (Tab. 2): (i) There is no significant coherence between the P-index and the projections of the relative vorticity advection by the zonally asymmetric time mean flow, χ_3, the self interaction among the low frequency eddies, χ_5, and the interaction between the low and high frequency eddies, χ_7. Therefore, these forcing terms cannot contribute to the amplification of the P-index. (ii) The term leading the P-index is due to the planetary vorticity advection by the low frequency flow, χ_1 with a phase of about 80°. In contrast, the projection of the relative vorticity advection by the zonal symmetric time mean flow, χ_2, lags the P-index by about 100°, and the divergence term, χ_4, lags the P-index by about 90°. Both terms, therefore, damp the P-index. (iii) The projections of the self interaction of the high frequency eddies, χ_6,

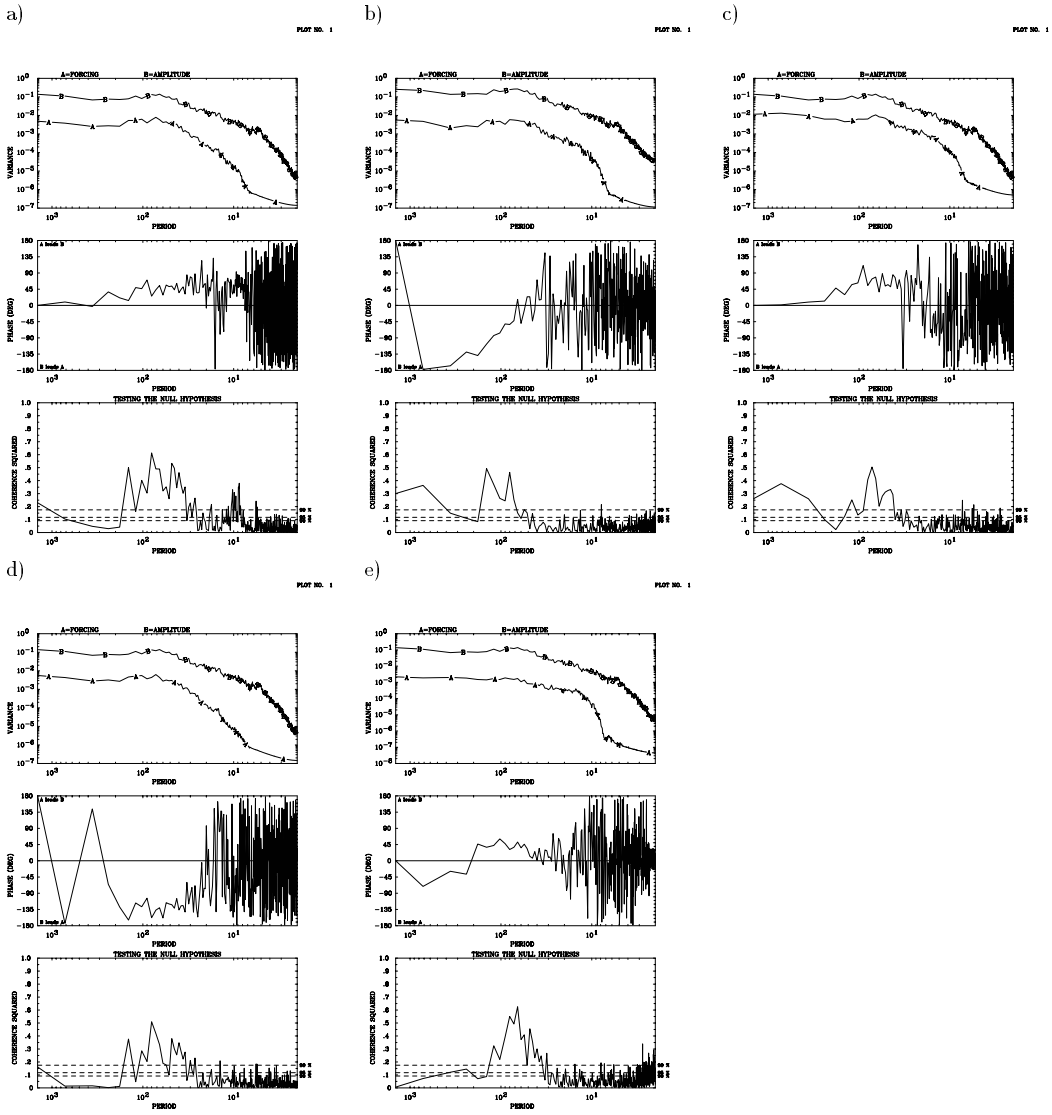

Figure 8. 150°-experiment (A-area): Spectral analysis of normalized scalar time series derived from projections of the forcing terms onto the A-pattern (curve A), and the A-index time series (curve B). Upper, middle and lower plot present the variance spectra, the phase spectra and the coherence squared for a) planetary vorticity advection by the low frequency flow, b) interaction between the zonal mean time mean flow with the low frequency flow, c) interaction between the zonally asymmetric time mean flow with the low frequency flow, d) the low frequency contribution to the divergence term, and e) the self interaction among the high frequency eddies.

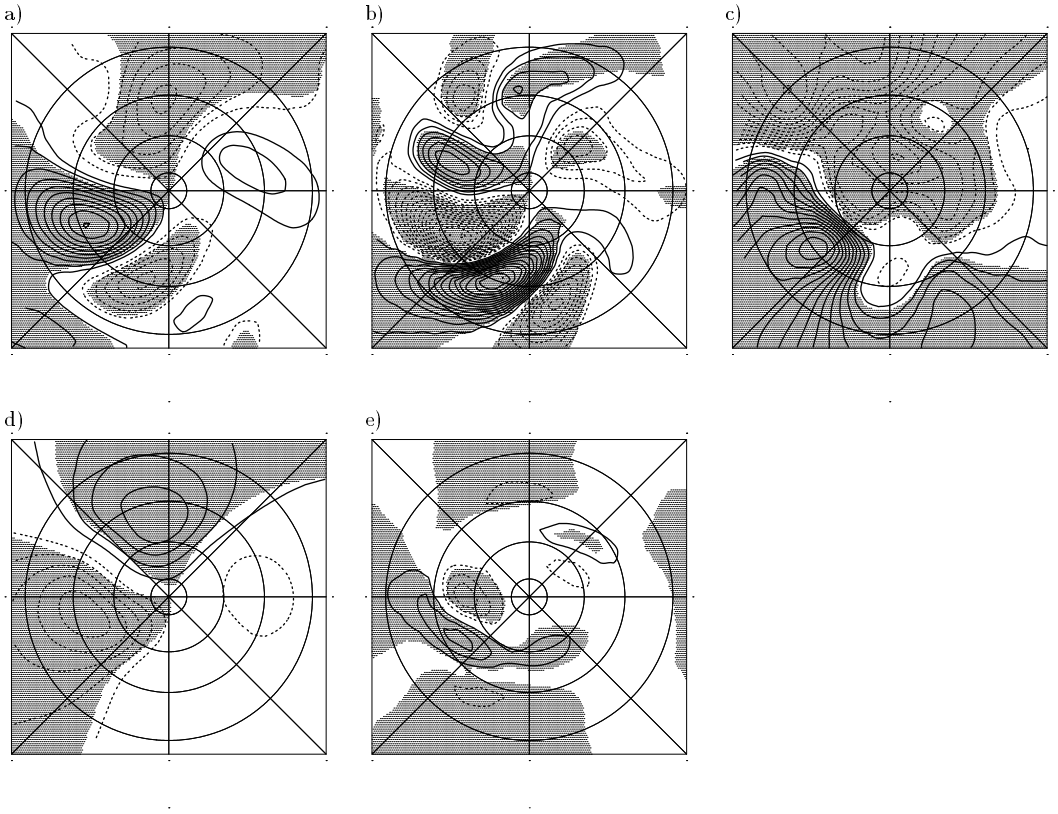

Figure 9. 150°-experiment (A-area): Composites for positive projections of A-index events at zero-lag (the zero contour is not displayed, shading indicates significance above the 99%-level): a) planetary vorticity advection by the low frequency flow (contour interval is $5m^2s^{-2}$), b) interaction between the zonal mean time mean flow with the low frequency flow (contour interval is $2m^2s^{-2}$), c) interaction between the zonally asymmetric time mean flow with the low frequency flow (contour interval is $2m^2s^{-2}$), d) the low frequency contribution to the divergence term (contour interval is $5m^2s^{-2}$), and e) the self interaction among the high frequency eddies (contour interval is $0.5m^2s^{-2}$).

lead the P-index by about 180° and, finally, the sum of the vertical vorticity advection and the tilting term, χ_8, is leading the P-index by about 170°. Thus both terms do not contribute to the P-index amplification due to their almost 180°-phase shift. Since the barotropic streamfunction tendency terms do not govern the time evolution of the P-index, baroclinic processes may play a more important role in its dynamics. This is analysed next.

(*c*) *Tendency of the quasi-stationary wave activity*

The dynamics underlying the P-pattern is analysed in terms of the budget of quasi-stationary wave activity, A_S, which is related to the potential enstrophy of the waves,

$$\frac{\partial A_S}{\partial t} + \nabla \cdot \vec{F}_S = C_S, \tag{8}$$

where C_S is the source due to local nonconservative and nonlinear processes. The (divergence of the) flux of quasi-stationary wave activity, $\vec{F}_S$ (Plumb 1985), identifies the

Barotropic forcing term	Dynamical process	Contribution	
		P-area	A-area
χ_1	planetary vorticity advection by low frequency flow	propagating	propagating
χ_2	interaction between zonal mean time mean flow and low frequency flow	attenuation	attenuation
χ_3	interaction between zonally asymmetric time mean flow and low frequency flow	none	amplifycation
χ_4	low frequency contribution to divergence term	attenuation	attenuation
χ_5	self interaction among the low frequency eddies	none	none
χ_6	self interaction among the high frequency eddies	none	amplifycation
χ_7	interaction between the low and high frequency eddies	none	none
χ_8	tilting terms plus vertical vorticity advection	none	none

TABLE 2. Forcing terms and their contribution in the A- and P-area..

source of baroclinic wave activity which, for stationary (but not necessarily steady) and quasi-geostrophic waves in a slowly varying zonal mean flow, is given by

$$\vec{F}_S = p \cdot cos\phi \begin{pmatrix} \frac{1}{2a^2 cos^2\phi}\left(\left(\frac{\partial\psi^\star}{\partial\lambda}\right)^2 - \psi^* \frac{\partial^2\psi^\star}{\partial\lambda^2}\right) \\ \frac{1}{2a^2 cos\phi}\left(\frac{\partial\psi^\star}{\partial\lambda}\frac{\partial\psi^\star}{\partial\phi} - \psi^* \frac{\partial^2\psi^\star}{\partial\lambda\partial\phi}\right) \\ \frac{2\Omega^2 sin^2\phi}{N^2 a \cdot cos\phi}\left(\frac{\partial\psi^\star}{\partial\lambda}\frac{\partial\psi^\star}{\partial z} - \psi^* \frac{\partial^2\psi^\star}{\partial\lambda\partial z}\right) \end{pmatrix}; \quad (9)$$

where Ω and a are the Earth's rotation rate and radius; λ, ϕ, z denote longitude, latitude, and the vertical component; N is the buoyancy frequency. For steady conservative waves $\vec{F}_S$ is non-divergent and, in the case of slowly varying almost plane waves, $\vec{F}_S$ is parallel to the group velocity (for further details see Plumb 1985, Black and Dole 1993, and Black 1997).

P-area: The space-time distribution of the anomalous stationary wave activity fluxes ($\vec{F}_S$ and its divergence) is displayed by lag-composites centered at maximum P-index (Fig. 10) with the maximum being centered at zero-lag: (i) *Before* zero-lag, a downstream (horizontal) flux of stationary wave activity emanates from the P-warm pole and the area of the upward (vertical) flux covers most of the entire storm track region (Fig. 10a and b). (ii) *At* zero-lag there is a downstream (horizontal) flux east of the center of the P-pattern where it converges with an upstream (horizontal) flux emanating from the A-cold pole (Fig. 10c). In addition, the positive or upward (vertical) flux amplifies and is shifted further downstream from the P-warm pole into the center of the P-pattern (Fig. 3d). The total flux-convergence in the center of the P-pattern leads to an accumulation of stationary wave activity enhancing its amplitude and, therefore, the P-index. (iii) *After* zero-lag, the P-index has reached its maximum the wave activity fluxes decreases considerably (Fig. 10e).

In summary, the high P-index events are characterized by an intense source of quasi-stationary wave activity. It induces a wave train, which emanates from the P-warm pole and propagates downstream across the P-storm track with maximum convergence of wave

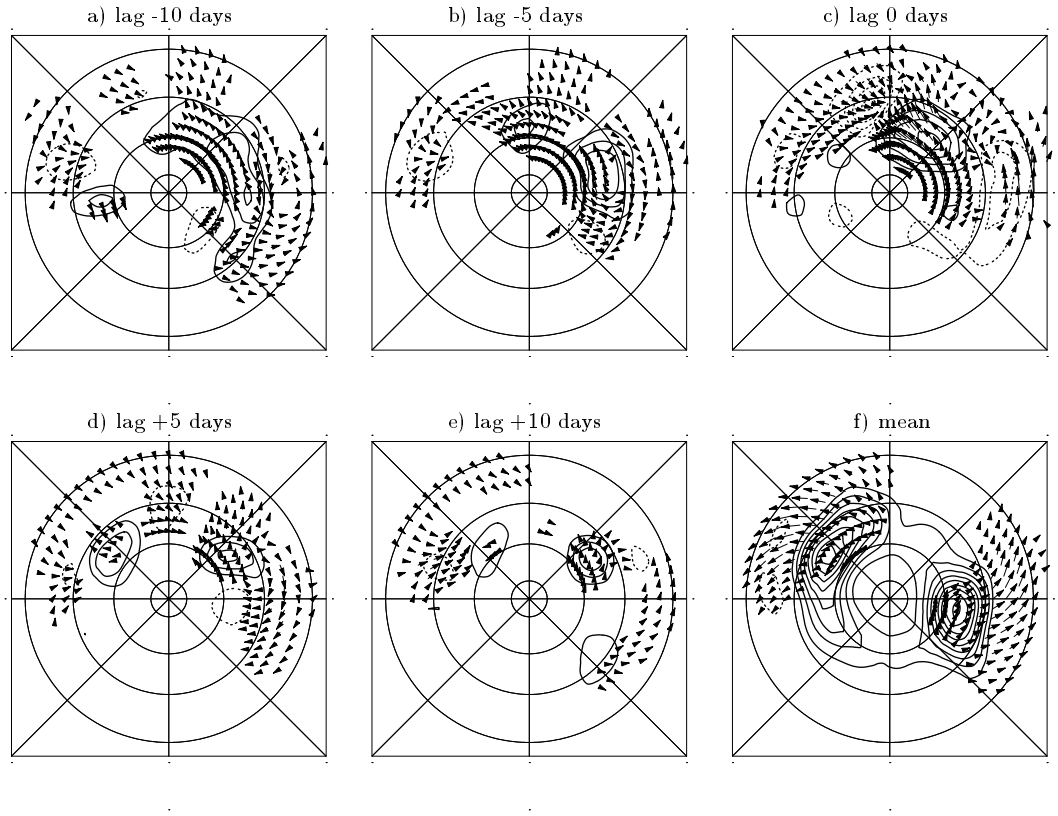

Figure 10. 150°-experiment (P-area): Composites of the anomalous stationary wave activity flux for positive projections of P-index events: a) day -10, b) day -5, c) day 0, d) day +5, e) day +10, f) time-mean. Vectors of the horizontal wave activity fluxes at 300 hPa are plotted over contours of the vertical part at 700 hPa, contour interval is 0.05 $m^2 s^{-2}$, positive (negative dashed) contours indicate an upward (downward) flux.

activity in its center. There the stationary wave activity is accumulated enhancing the stationary wave amplitude (and, therefore, the P-index). The accumulation is further enhanced by the upstream propagation of wave activity originating from the A-cold pole situated downstream. The composite analysis of the stationary wave activity flux patterns reveals the importance of baroclinic wave sources for the anomaly in the P-area.

5. Summary and conclusions

Idealized experiments are carried out, in which the zonal distance between two mid-latitude storm tracks is reduced from 180° to 130° to analyse teleconnection patterns and low frequency variability. The area downstream of the shifted T_R-dipole is called the A-area, the other one P-area. With reference to the Atlantic and Pacific storm tracks of the Northern Hemisphere, the A- and P-indices and their patterns are defined in the respective areas. In the 180°-experiment the teleconnection patterns describe the retrograde travelling Rossby wave number two (Franzke et al. 2000). For a more realistic 150°-storm track separation the following results are obtained:

The teleconnection patterns (that is, the A- and P-pattern) are similar to the NAO and the PNA found in observations (e.g. Wallace and Gutzler 1981). This indicates that the global stationary wave field interacting with the storm tracks is to a large amount responsible for the regional spatial patterns of low frequency variability. The importance of the stationary waves for the location of low frequency patterns is also pointed out by Branstator (1990); Kang (1990) shows that the responses of forced Rossby waves depend strongly on the structure of the zonal mean flow. Lag-correlation patterns derived from low pass filtered data suggest a Rossby wave dispersion with a predominance of southward dispersion from the midlatitudes into the tropics. A similar behaviour is reported for intermediate (10-30 day periods) time scales in an observational study (Blackmon et al. 1984b).

The daily teleconnection index time series reveals that, with decreasing zonal separation of the two storm tracks, the correlation between the A-index and the P-index tends to zero. While the correlation is significant and remains roughly unaltered between 180° and 165°, it tends to zero from 155° to 130° separation. That is, there is a transition from a global zonal wavenumber two regime, as described in Franzke et al. (2000), to localized structures in the two storm track regions which are uncorrelated with one another. Bongionannini-Cerlini et al. (1999) find monthly PNA and NAO index time series being anti-correlated (-0.42); this, however, could be due to the trend in their time series, which is absent in the 150°-experiment. Analysing blocking event indices they confirm Lejenäs and Økland (1983), that the Pacific and the Atlantic sector are not correlated. Also, our analysis does not reveal the existence of zonal symmetric modes (like the Arctic Oscillation, Thompson and Wallace 1998) which, however, could be due to the course vertical resolution of the model, missing the stratosphere-troposphere link.

As both A- and the P-patterns exist in the $140° - 155°$ range of zonal T_R-dipole separations, we assume that the underlying dynamical processes are similar. The dynamical analysis identifies two different mechanisms describing the life cycles of the anomalies, which characterize the A- and P-index variability and their respective teleconnection patterns in the 150°-experiment:
A-index mechanism: A retrograde travelling Rossby wave is responsible for the low frequency variability in the A-region. It is induced by the interaction between the zonally asymmetric time mean flow (stationary wave) with the low frequency flow. That is, the interaction between the zonally asymmetric time mean flow and the low frequency flow supported by observational and other studies (see Frederiksen 1983, Simmons et al. 1983, Branstator 1992, Feldstein 1998 and 2000) excites the low frequency anomalies; the high frequency eddies help to maintain them through the 'spatial resonance' mechanism (Franzke et al. 2000). And, finally, the decay of the anomaly is due to the interaction between the zonal mean time mean flow with the low frequency flow, and the low frequency contribution to the divergence term (see also Feldstein 1998).
P-index mechanism: A stationary wave and the associated baroclinic wave sources are responsible for the low frequency variability in the P-region. Local baroclinic wave sources excite and maintain the P-pattern. Furthermore, there is an influence of the A-area on the formation of the P-pattern which is realized by the horizontal flux of wave activity emanating from the A-cold pole into the center of the P-pattern. That is, the zonal limitation of the P-area is responsible for the more wave-like structure of its teleconnection pattern, contrasting the longer zonal extension of the A-area with its zonally elongated pattern. This is supported by observations of persistent flow anomalies associated with the PNA and the Eastern Atlantic pattern. Black (1997) finds that, during anomaly life cycles, marked upward and downstream fluxes of wave activity occur locally; that is,

the primary wave sources originate where the anomalies appear. Furthermore, baroclinic conversions play an important role during the development of persistent negative height anomalies over the North Pacific Ocean (similar to the PNA-pattern; Black and Dole 1993), which is followed by increasing (decreasing) barotropic (baroclinic) contributions to the growth of the anomalies (Dole and Black 1990).

Acknowledgement

Thanks are due to Katrin Walter, Ute Luksch and Christoph Raible for stimulating discussions. The detailed and helpful comments by Steven Feldstein and another anonymous reviewer are very much appreciated. The research was funded by the Bundesministerium für Bildung und Forschung (07 KFT 1211), the Deutsche Forschungsgemeinschaft (SFB 512), and the Deutscher Akademischer Austauschdienst and the National Science Foundation (315/PPP/ab).

References

Black, R. X.	1997	Deducing Anomalous Wave Source Regions during the Life cycles of Persistent Flow Anomalies. *J. Atmos. Sci.*, **54**, 895–907
Black, R. X., and Dole, R. M.	1993	The Dynamics of Large-Scale Cyclogenesis over North Pacific Ocean. *J. Atmos. Sci.*, **50**, 421–442
Blackmon, M. L.	1976	A climatological spectral study of the 500 mb geopotential height of the Northern Hemisphere. *J. Atmos. Sci.*, **33**, 1607–1623
Blackmon, M. L., Lee, Y.-H. and Wallace, J. M.	1984a	Horizontal structure of 500 mb height fluctuations with long, intermediate and short time scales. *J. Atmos. Sci.*, **41**, 961–979
Blackmon, M. L., Lee, Y.-H., Wallace, J. M. and Hsu, H.-H.	1984b	Time variation of 500 mb height fluctuations with long, intermediate and short time scales as deduced from lag-correlation statistics. *J. Atmos. Sci.*, **41**, 981–991
Bongioannini-Cerlini, P., Corti, S. and Tibaldi, S.	1999	An intercomparision between low frequency variability indices. *Tellus*, **51**, 773–789
Branstator, G. W.	1990	Low-frequency patterns induced by stationary waves. *J. Atmos. Sci.*, **47**, 629–648
Branstator, G. W.	1992	The maintenance of low-frequency atmospheric anomalies. *J. Atmos. Sci.*, **49**, 1924–1945
Cai, M. and van den Dool, H. M.	1994	Dynamical decomposition of low-frequency tendencies. *J. Atmos. Sci.*, **51**, 2086–2100
Dole, R. M., and Black, R. X.	1990	Life cycles of persistent anomalies. Part II: The development of persistent negative height anomalies over the North Pacific ocean. *Mon. Wea. Rev.*, **118**, 824–846
Feldstein, S. B.	1998	The growth and decay of low-frequency anomalies in a GCM. *J. Atmos. Sci.*, **55**, 415–428
Feldstein, S. B.	2000	Fundamental mechanisms of PNA growth and decay. *J. Climate*, , submitted
Fraedrich, K., Bantzer, C. and Burkhardt, U.	1993	Winter climate anomalies in Europe and their associated circulation at 500 hPa. *Climate Dyn.*, **8**, 161–175
Fraedrich, K., Kirk, E., and Lunkeit, F.	1998	Portable University Model of the Atmosphere. *Technical Report 16, Deutsches Klimarechenzentrum*, 37pp., available at: http://www.dkrz.de/forschung/reports.html
Franzke, C., Fraedrich, K. and Lunkeit, F.	2000	Low frequency variability in a simplified atmospheric global circulation model: Storm track induced 'spatial resonance'. *Q. J. R. Meteorol. Soc.*, **126**, 2691–2708

Frederiksen, J. S. 1983 A unified three dimensional instability theory of the onset of blocking and cyclogenesis. II: Teleconnection patterns. *J. Atmos. Sci.*, **40**, 2593–2609

Frisius, T., Lunkeit, F., Fraedrich, K. and James, I. N. 1998 Storm-track organization and variability in a simplified atmospheric global circulation model. *Q. J. R. Meteorol. Soc.*, **124**, 1019–1043

Held, I. M. and Suarez, M. J. 1994 A proposal for the intercomparison of the dynamical cores of atmospheric general circulation models. *Bull. Amer. Meteorol. Soc.*, **75**, 1825–1830

Hoskins, B. J. and Simmons, A. J. 1975 A multi-layer spectral model and the semi-implicit method. *Q. J. R. Meteorol. Soc.*, **101**, 637–655

James, I. N. and Gray, L. J. 1986 Concerning the effect of surface drag on the circulation of a planetary atmosphere. *Q. J. R. Meteorol. Soc.*, **112**, 1231–1250

James, I. N. and James, P. M. 1992 Spatial structure of ultra low frequency variability of the flow in a simple atmospheric circulation model. *Q. J. R. Meteorol. Soc.*, **118**, 1211–1233

James, P. M., Fraedrich, K. and James, I. N. 1994 Wave zonal flow interaction and ultra low frequency variability in a simplified global circulation model. *Q. J. R. Meteorol. Soc.*, **120**, 1045–1067

Kang, I.-S. 1990 Influence of Zonal Mean Flow on Stationary Wave Fluctuations. *J. Atmos. Sci.*, **47**, 141–147

Lau, N.-C. 1988 Variability of the observed midlatitude stormtracks in relation to low frequency changes in the circulation pattern. *J. Atmos. Sci.*, **45**, 2718–2743

Lejenäs, H., and Økland, H. 1983 Characteristics of northern hemisphere blocking as determined from a long time series of observational data. *Tellus*, **35**, 350–362

Lunkeit, F., Fraedrich, K. and Bauer, S. E. 1998 Storm tracks in a warmer climate: sensitivity studies with a simplified global circulation model. *Climate Dyn.*, **14**, 813–826

Plaut, G. and Vautard, R 1994 Spells of low frequency oscillations and weather regimes in the northern hemisphere. *J. Atmos. Sci.*, **51**, 210–236

Plumb, R. A. 1985 On the Three-Dimensional Propagation of Stationary Waves. *J. Atmos. Sci.*, **42**, 217-229

Sickmöller, M., Blender, R. and Fraedrich, K. 2000 Observed winter cyclone tracks on the Northern Hemisphere in re-analysed ECMWF-data. *Q. J. R. Meteorol. Soc.*, **126**, 591-620

Simmons, A. J., Wallace, J. M. and Branstator, G. W. 1983 Barotropic wave propagation, and instability, and atmospheric teleconnection patterns. *J. Atmos. Sci.*, **40**, 1363–1392

Thompson, D. W. J., and Wallace, J. M. 1998 The Arctic Oscillation signature in the wintertime geopotential height and temperature fields. *Geophys. Res. Lett.*, **25**, 1297–1300

Trenberth, K. E. 1991 Storm tracks in the southern Hemisphere. *J. Atmos. Sci.*, **48**, 2159–2178

von Storch, H. and Zwiers, F. W. 1998 *Statistical analysis in climate research.*, Cambridge University Press, Cambridge, 510 pp.

Wallace, J. M. and Gutzler, D. S. 1981 Teleconnections in the geopotential height field during the Northern Hemisphere winter. *Mon. Weather Rev.*, **109**, 785-812

Walter, K., Luksch, U. and Fraedrich, K. 2000 A response climatology of idealized SST anomaly experiments with and without storm track. *J. Climate*, in press